ACS OMEGA

http://pubs.acs.org/journal/acsodf

Article

Effect of Optimized Precursor Concentration, Temperature, and Doping on Optical Properties of ZnO Nanoparticles Synthesized via a Green Route Using Bush Tea (*Athrixia phylicoides* DC.) Leaf Extracts

Amani Gabriel Kaningini, Shohreh Azizi,* Nolufundo Sintwa, Kagiso Mokalane, Keletso Cecilia Mohale, Fhatuwani Nixwell Mudau, and Malik Maaza

Cite This: *ACS Omega* 2022, 7, 31658−31666

Read Online

ACCESS | Metrics & More | Article Recommendations

ABSTRACT: Nanoparticles possess several properties, such as antimicrobial, anti-inflammatory, wound healing, catalytic, magnetic, optical, and electronic properties, that have allowed them to be used in different fields. Among them, zinc oxide (ZnO) has received copious consideration due to its technological and medicinal applications. Plant-mediated synthesis of ZnO nanoparticles has provided a cost-effective and eco-friendly method. Therefore, the objective of the study is to assess the effect of the precursor concentration and silver and cerium doping on the optical properties of ZnO nanoparticles synthesized via a green process using bush tea leaf extract as the chelating agent. Zinc nitrate hexahydrate was used as the precursor. Quasi-spherical-shaped ZnO nanoparticles were obtained with an average crystallite size ranging between 24.53 and 63.02 nm. The crystallite size was found to decrease with the increase of precursor concentration at 43.82 nm (0.05 g), 37.25 nm (0.10 g), 26.53 nm (0.50 g), and 24.53 nm (1 g); thereafter, the size increases with an increase in precursor concentration. The optimum precursor concentration was 1 g with the smallest grain size and a high purity level. The increase in annealing temperature induced an increase in the crystallite size of ZnO nanoparticles from 24.53 nm (600 °C) to 34.24 nm (800 °C), however, increasing the level of purity of the nanopowders. The band gap energies were 2.75 and 3.17 eV as calculated using the Tauc plot with variations due to the precursor concentrations. Doping with both silver and cerium increased the band gap of ZnO nanoparticles up to 3.19 eV and the increase in annealing temperature slightly augmented the band gap energy from 3.00 and 3.16 eV, respectively. Hence, doping with Ag and Ce induced the formation of nanorods at higher concentrations. This study successfully demonstrated that the natural plant extract of bush tea can be used in the bioreduction of zinc nitrate hexahydrate to prepare pure ZnO nanoparticles, thus extending the use of this plant to the nano producing industry.

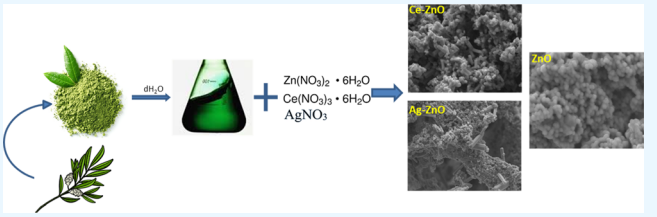

1. INTRODUCTION

Zinc oxide (ZnO) nanomaterials are globally synthesized for their various properties, such as antimicrobial, anti-inflammatory, wound healing, catalytic, magnetic, optical, and electronic properties, that have put them at the forefront of a wide variety of studies, allowing researchers to use them in biosensing and energy generation devices as well as for different drug deliveries for the treatment of various illnesses such as cancer.[1−3] Nanomaterials' physical, chemical, magnetic, electrical, and optical characteristics can change considerably from their bulk counterparts due to their high surface area to volume ratio.[4]

The synthesis of metal oxides, such as ZnO, has been done through various chemical and physical methods to date.[5] However, the variation in concentrations of the precursor, as well as the medium of synthesis, can affect the morphology and other significant properties of the obtained nanoparticles.[6,7] Hence, the effect of precursor concentration on the properties of nanoparticles are reported lightly.[7]

In recent research, great progress has been made in the engineering of ZnO-based devices that require band gap engineering for adjustment to the different uses.[8] ZnO has a large direct band gap of 3.37 eV and a high exciton binding energy of 60 meV.[4] The band gap engineering of ZnO nanomaterials is achieved through doping with other metals and rare earth such as Mn, Ce, Fe, Eu, Er, Co, and Tb.[8,9] Behrens et al. reported that the increase in Al levels reduces the band gap energy of ZnO nanoparticles when the doped amount does not exceed 4 mol %.[10] The same trend has been

Received: January 31, 2022
Accepted: March 28, 2022
Published: August 29, 2022

observed with Mg^{2+} doping. Mg-doped ZnO nanoparticles were found to have a band gap energy of 3.04 eV.[11]

The introduction of living systems in the synthesis of nanoparticles has been reported as a safe and eco-friendly way of synthesizing various metal nanoparticles.[1,12,13] Various plants containing flavonoids such as naringin, diosmin, quercetin, and hesperidin have been used in the production of nanoparticles.[14,15] Bush tea is a well-known South African indigenous herbal tea that has been used for decades for treating various ailments.[16] This aromatic shrub and indigenous tea plant from the Asteraceae family was found to possess several compounds such as polyphenols and flavonoids that are associated with antioxidants, antimicrobial, and anti-inflammatory activities.[17,18] Flavonoids and phenols have been used in several studies for the synthesis of nanoparticles such as silver,[19] gold,[20] and zinc.[21] Due to the lack of information regarding the effect of doping and precursor concentration on ZnO nanoparticles' optical properties synthesized by a green route using plants, this study aims to characterize ZnO, Ag−ZnO, and Ce−ZnO nanoparticles synthesized using *Athrixia phylicoides* DC leaf extract as a reducing agent.

2. EXPERIMENTAL PROCEDURE

2.1. Material Preparation. Bush tea leaves were harvested from the wild in the city of Thohoyandou (22.8785°S; 30.4818°E), Limpopo province, South Africa. After harvest, the leaves were thoroughly washed with deionized water and freeze-dried at −50 °C for 72 h then ground into a powder. For extraction, 10 g of leaf powder was weighed and mixed with 300 mL of deionized water. The mixture was heated at 60 °C until the water turned to a dark green color and then cooled down at room temperature. After centrifugation at 4000 rpm for 10 min using a Beckman Allegra X-30 centrifuge, the mixture was filtered twice using a Whatman no 1 filter paper and the extract was kept in an airtight container. An analytical grade zinc nitrate hexahydrate $\{[Zn(NO)_3]_2{\cdot}6H_2O\}$ purchased from Sigma-Aldrich South Africa was used as the precursor.[22]

2.2. Synthesis of ZnO, Ag−ZnO, and Ce−ZnO. *2.2.1. Precursor Optimization.* Different concentrations of zinc nitrate hexahydrate (0.05, 0.1, 0.5, 1, 2, 3, 4, and 5 g) were singularly mixed with 25 mL of bush tea extract. The mixture was kept under a vigorous magnetic stirrer 200 rpm at ≈80 °C until a dark-colored paste was observed. The paste was then cooled down at room temperature and annealed at 600 °C and a yellowish powder was obtained.

2.2.2. Temperature Optimization. After selection of the optimum precursor concentration (1 g), the synthesis process was repeated using 1 g of zinc nitrate hexahydrate and 25 mL of bush tea extract in two different crucible tubes. The mixture was kept under 200 rpm at ≈80 °C until a dark-colored paste was observed. The paste was then cooled down at room temperature and annealed at 600 and 800 °C to reduce the impurities.

2.2.3. Silver and Cerium Doping. Cerium nitrate hexahydrate and silver nitrate were used as dopants of ZnO nanoparticles. After the selection of the optimum temperature (800 °C) and precursor concentration (1 g), 1 and 2% equiv mol of $Ce(NO_3)_3$ and $AgNO_3$ were weighed and added to the solution containing 1 g of precursor and 25 mL of bush tea extract in four different beakers. The mixture was then subjected to the synthesis process as mentioned above and was annealed at 800 °C.

2.2.4. Material Characterization. The properties of the obtained ZnO powders were investigated by various characterization techniques. For the structure determination, a field emission scanning electron microscope was used at a beam energy of 20 kev. A Thermo Scientific energy-dispersive spectrometer was used to determine the elemental composition of the powder samples. The Brucker AXS D8 ADVANCE X-ray diffractometer with Cu Kα radiation and wavelength, $\lambda(K\alpha_1)$ = 1.5406 Å was used to obtain the phase and structural identification of nanoparticles. A frontier Fourier transformed infrared (FTIR) spectrometer was used to evaluate the composition quality of nano-powders. Also, a PerkinElmer ultraviolet−visible (UV−vis) LAMBDA 650S spectrometer was used to measure the optical properties of the nanoparticles.

3. RESULTS AND DISCUSSION

3.1. X-ray Diffraction. Figure 1 shows the X-ray diffraction (XRD) pattern of the powders synthesized using different concentrations of the precursor. All the samples presented peaks at 32, 34, 36, 47, 56, 63, 66, 68, 69, 73, and 77° corresponding to the Wurtzite structure of ZnO nanoparticles (ICDD # 897102). Other peaks were identified at 28, 31, 41, and 51° disappear as the precursor concentration increases and are attributed to the presence of KCl, K_2SO_4, and $KZnO_2$ in the powders as a result of K, S, and Cl ions present in the natural composition of *A. phylicoides* DC.[23] Using the Scherrer equation,[24] the crystallite size of the obtained crystals was ranging between 24.53 and 63.02 nm. The increase in precursor concentration reduced the crystallite size of the obtained nanoparticles at 0.05, 0.1, 0.5, and 1 g of the precursor was found to be 43.82, 37.25, 26.53, and 24.53 nm, respectively. However, from 1 g of the precursor, an increase in precursor concentration induces the increase of the crystallite size of the ZnO nanoparticle, providing that 1 g of the precursor is the optimum concentration. The average crystallite size of particles using 5 g of the precursor was found to be 63.02 nm. According to Pholnak et al. (2014), the variations in precursor concentration significantly impacts the purity and crystallinity of the ZnO nanoparticles.[6]

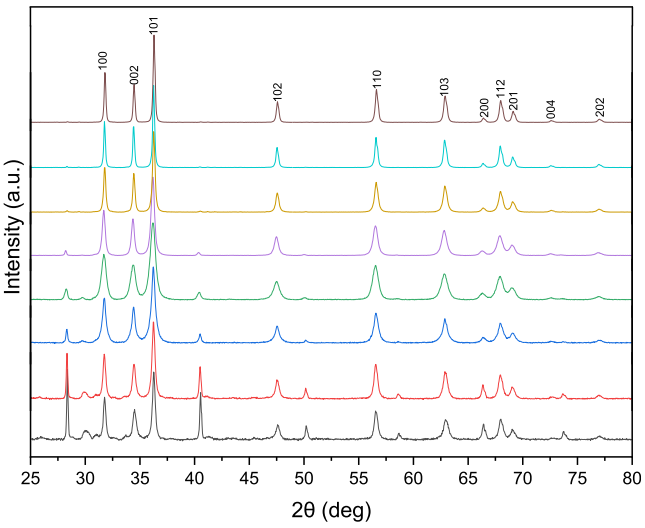

Figure 1. XRD pattern of ZnO nanoparticles synthesized using different concentrations of the precursor.

https://doi.org/10.1021/acsomega.2c00530
ACS Omega 2022, 7, 31658−31666

The variation in the annealing from 600 to 800 °C has induced the disappearance of several peaks considered as resulting from a remanent excess of the exact in the ZnO powders. The peaks found at 28, 31, 41, and 51° identified as the signature of K, S, and Cl are not visible at annealing temperature 800 °C (Figure 2). With the increase of the annealing temperature, the crystallite size varies from 24.53 to 34.24 nm. The crystallite size of ZnO nanoparticles has improved with the increase of the annealing temperature. These findings concur with the study of Uthirakumar and Hong (2009) who reported that higher annealing temperatures improve the crystal quality of ZnO nanoparticles inducing a reduction of the full-width half-maximum value.[25]

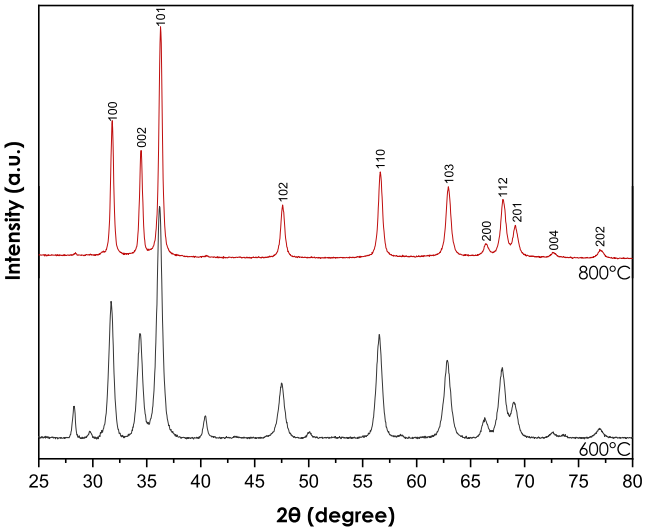

Figure 2. XRD pattern of ZnO nanoparticles annealed at different temperatures.

The powders obtained after doping with Ce and Ag show sharp peaks related to the high crystallinity of ZnO particles. The slight shift in the peak position after doping ZnO nanoparticles with Ce (Figure 3) to a higher 2θ was observed with the increase of dopant concentration. This might have been caused due to the replacement of Zn^{2+} ions with a lower radius (0.074 nm) by Ce^{3+} ions with a larger radius (0.103 nm) causing a local strain in the ZnO lattice.[26] The crystallite size of Ce-doped ZnO nanoparticles was found to be decreasing with the augmentation of the doping concentration, 32.17 and 30.33 nm when using 1 and 2% of the dopant, respectively.

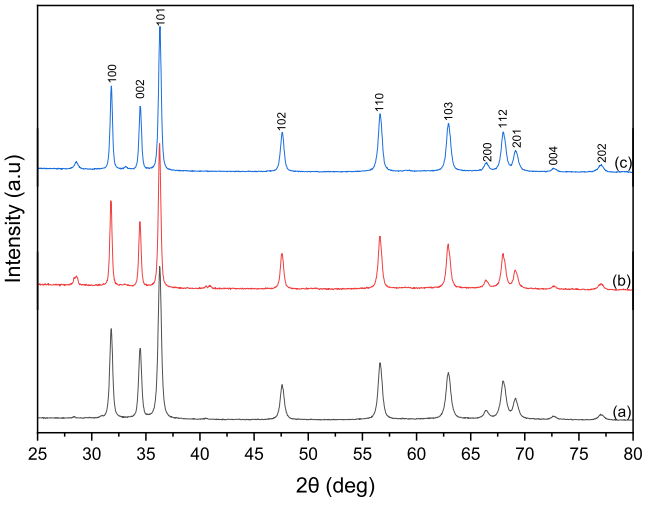

Figure 3. XRD pattern of (a) pure and (b) 1% Ce-doped and (c) 2% Ce-doped ZnO nanoparticles.

The XRD pattern of ZnO nanoparticles doped with Ag is presented in Figure 4. No peak shift was observed to confirm a certain surface doping or segregation of Ag nanoclusters on the grain boundaries of ZnO nanoparticles.[27] However, doping with Ag considerably reduced the crystallite size of ZnO nanoparticles that was 25.51 and 20.89 nm, respectively, for 1 and 2%, hence the size was found to decrease with the increase in dopant concentration. Several Ag peaks appear at 27, 28, 40, 46, 54, and 57°. Their intensity increases with the increase of dopant concentration. These peaks could be attributed to the metallic second phase of Ag in formation.[28]

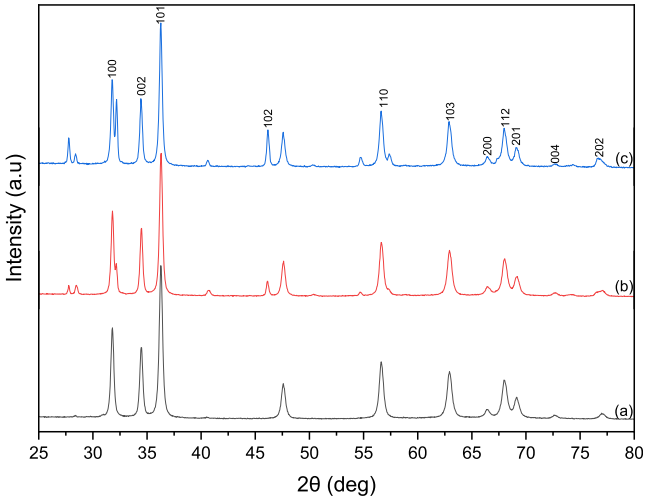

Figure 4. XRD pattern of (a) pure and (b) 1% Ag-doped and (c) 2% Ag-doped ZnO nanoparticles.

3.2. Fourier Transformed Infrared. The FTIR spectra of ZnO powders synthesized using different concentrations of the precursor are presented in Figure 5. Different absorption peaks were detected in the range 4000−400 cm^{-1}. The broad absorption peak observed between 3735 and 3023 cm^{-1} corresponds to the O−H stretching of the intramolecular hydrogen bond. The reduction of precursor concentrations was decreasing the intensity of the peak attributed to the O−H bond. The peaks observed at 1691 to 1611 cm^{-1} correspond to the C═C stretching of the alkene group. The peak observed at 2346 cm^{-1} is present only when the concentrations of the precursor are too low (0.1 and 0.05 g); they might be attributed to the absorption of atmospheric CO_2 on the metallic cations, probably present in the apparatus during analysis. The absorption band of the wurtzite ZnO in the range 400−500 cm^{-1} is the strongest in the case of single-phase ZnO.[6]

With the increase in annealing temperature (Figure 6), the C≡C stretching peak at 1691 cm^{-1}, which is attributed to the stretching bond of the alkene group, disappears. The ZnO stretching mode is responsible for the sharp peak at 400−500 cm^{-1}. However, the rising of the annealing temperature deteriorates the ZnO peak.[29] The presence of ambient CO_2 in the apparatus during the analysis might explain the CO_2 peak at 2348 cm^{-1}.

https://doi.org/10.1021/acsomega.2c00530
ACS Omega 2022, 7, 31658−31666

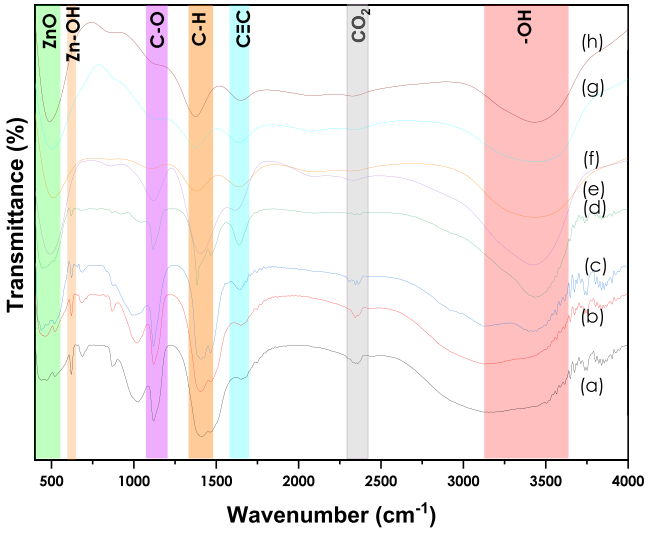

Figure 5. FTIR spectra of ZnO nanoparticles synthesized using different concentrations of precursor: (a) 0.05, (b) 0.1, (c) 0.5, (d) 1, (e) 2, (f) 3, (g) 4, and (h) 5 g.

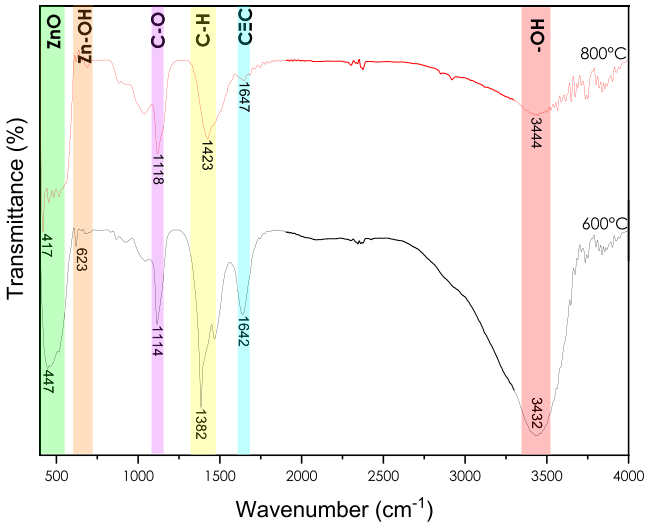

Figure 6. FTIR spectra of ZnO nanoparticles annealed at 600 and 800 °C.

The doping effect of cerium on ZnO nanoparticles is presented in Figure 7. There is the appearance of a new peak at 2348 cm^{-1} due to the atmospheric CO_2 present in the apparatus during analysis. The observation shows that doping with cerium the broad peak at 3453 cm^{-1} due to the stretching mode of the O−H group and the one at 1634 cm^{-1} which is allocated to the stretching of C═C in the aromatic ring or C═O in polyphenols broaden with the increase of the dopant concentration.[26] The starching peak related to the Ce−ZnO was observed between 250 and 500 cm^{-1} confirming the integration of Ce^{3+} ions in the ZnO lattice.

Doping ZnO with silver nitrate (Figure 8) creates a slight shift of the ZnO peak. The shift can be associated with the substitution of Ag^{+} ions in the ZnO lattice.[28] A sharp peak is observed at 2344 cm^{-1} due to the presence of atmospheric CO_2 in the apparatus during analysis. Other peaks observed were observed in the pure ZnO powders.

3.3. Scanning Electron Microscopy. The field emission scanning electron microscopy (FE-SEM) images of particles

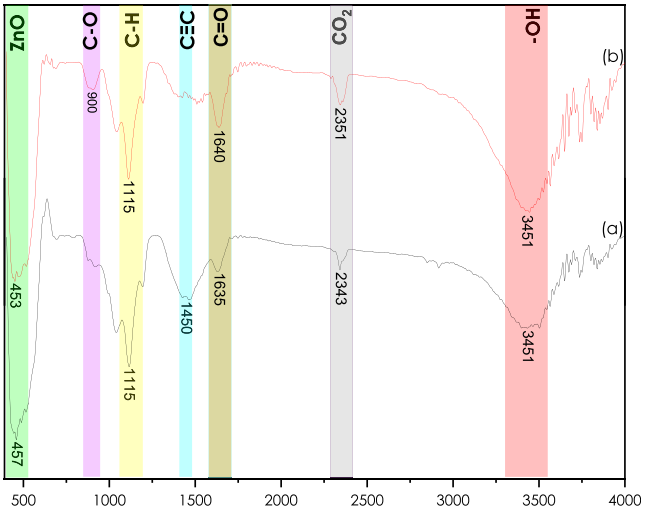

Figure 7. FTIR spectra of ZnO nanoparticles doped with (a) 1 and (b) 2% of cerium nitrate.

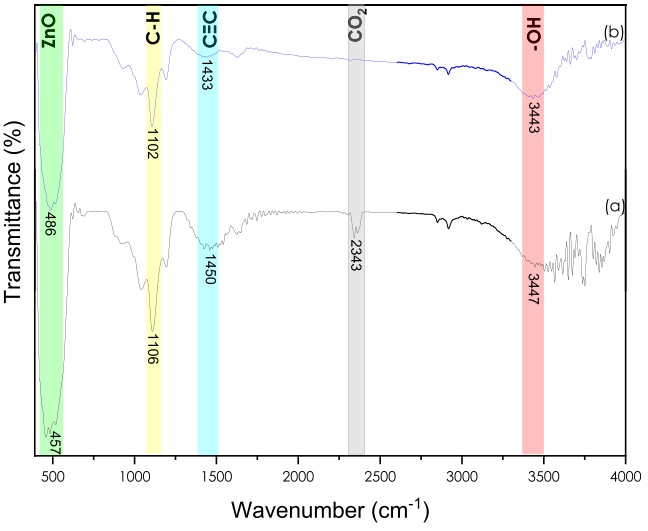

Figure 8. FTIR spectra of ZnO nanoparticles doped with (a) 1 and (b) 2% of silver.

from low precursor concentrations show spherical-shaped ZnO nanoparticles agglomerated together as presented in Figure 9. The agglomeration seems to increase with the increase in precursor concentration, hence keeping the spherical shape of particles. The agglomeration might be due to the polarity and electrostatic attraction of ZnO nanoparticles biologically synthesized.[30] However, at higher concentrations (4 and 5 g of precursor) the spherical shape of ZnO nanoparticles is mixed with hexagonal and cubical grains (Figure 9g,h). The increase of precursor concentration lowers the rearrangement of nanoparticles and decreases their homogeneity.[31]

The FE-SEM images of ZnO nanoparticles doped with Ce are presented in Figure 10. Results show that with lower concentrations of dopant the samples have spherical ZnO nanoparticles with a high monodispersion (Figure 10a). The increase in dopant concentration (Figure 10b) induces the formation of nano-rods that appear to be predominant, however monodispersed. It is well-known that Ce plays an important role in ZnO capping and prevents the aggregation between particles due to its hindrance effect.[26]

https://doi.org/10.1021/acsomega.2c00530
ACS Omega 2022, 7, 31658−31666

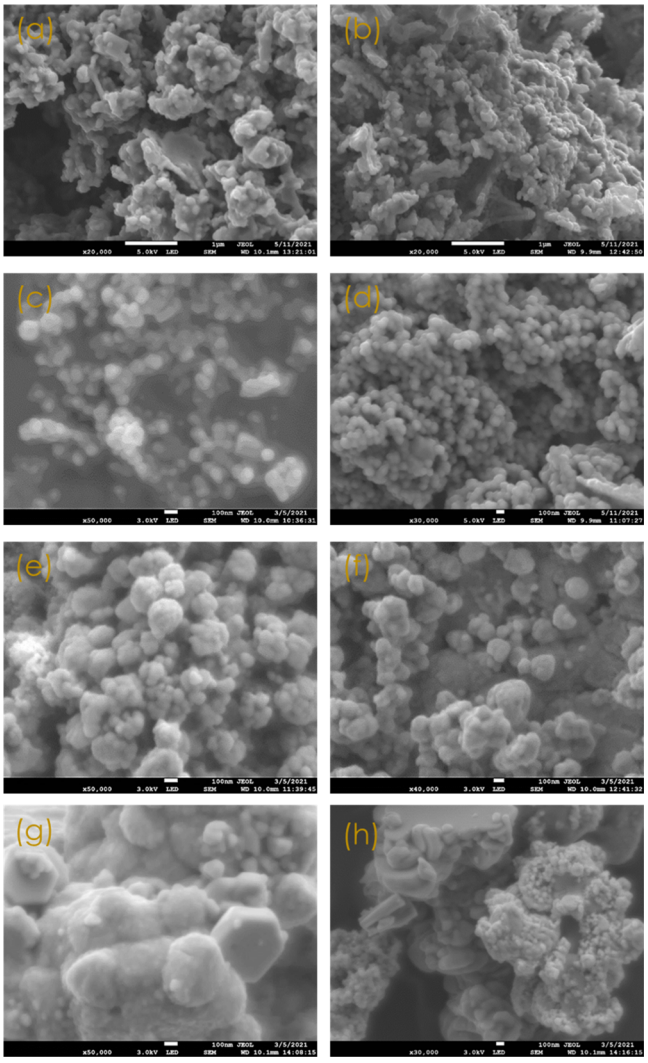

Figure 9. SEM image of ZnO nanoparticles synthesized using (a) 0.05, (b) 0.1, (c) 0.5, (d) 1, (e) 2, (f) 3, (g) 4, and (h) 5 g of the precursor.

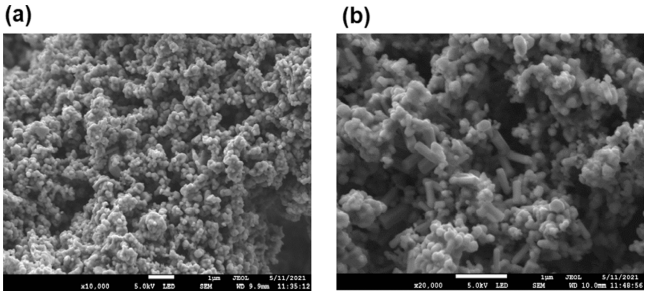

Figure 10. SEM images of (a) 1 and (b) 2% Ce-doped ZnO nanoparticles.

The FE-SEM images of Ag-doped ZnO nanoparticles (Figure 11) present quasi-spherical nanoparticles clustered together (Figure 11a) at concentration 1%. The increase in dopant concentration up to 2% induces the formation of nanorods (Figure 11b). However, the size distribution of nanoparticles was found to be uniform.

3.4. Energy-Dispersive X-ray Spectroscopy. The energy-dispersive spectrometry (EDS) spectra shown in Figure 12 have confirmed the presence of Zn and O with broad peaks

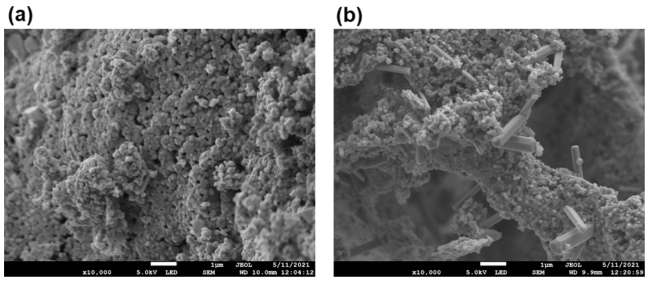

Figure 11. SEM images of (a) 1 and (b) 2% Ag-doped ZnO nanoparticles.

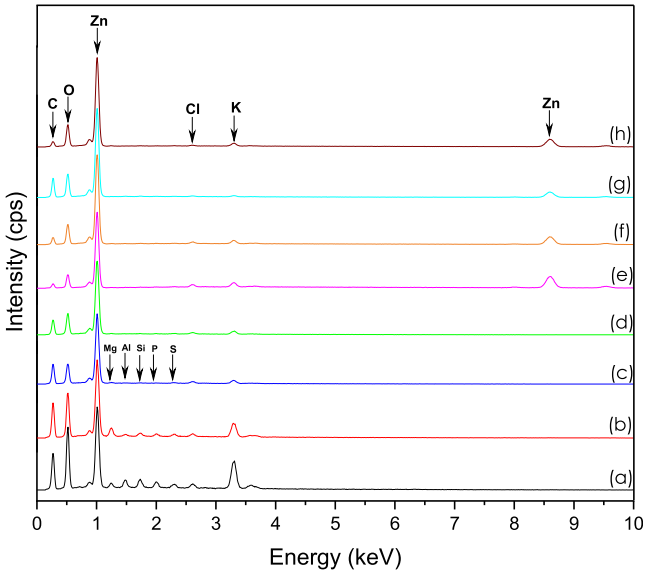

Figure 12. EDS spectra of ZnO nanoparticles synthesized using different precursor concentrations (a) 0.05, (b) 0.1, (c) 0.5, (d) 1, (e) 2, (f) 3, (g) 4, and (h) 5 g.

that increase with the precursor concentration. Different traces were found in the powders such as Cl, Si, S, and K. These peaks attributed to the natural extract are reduced with the increase of precursor concentration until they start to disappear from 1 g of precursor. Only the K and Cl peaks remain. Much more pure powders were observed using 1 g of precursor with some traces of K. Another peak that was observed was from the carbon tube used for coating.

The EDS data presented in Figure 13 show the presence of zinc and oxygen in both Ce-doped and Ag-doped samples. A cerium peak was observed with the increase of dopant concentration to 2% due to its nonintegration into the ZnO lattice. A persistent Cl peak that could be from the extra plant material was observed. The C peak is a result of coating. Ag-doped ZnO nanoparticles present several Ag peaks, and the presence of K and Cl is observed in both samples, suggesting that Ag did not integrate completely in the ZnO lattice.

3.5. Ultraviolet−Visible Spectroscopy. The UV−vis spectra of ZnO nanoparticles synthesized using different concentrations of the precursor were recorded using a UV−vis spectrometer in the wavelength 250−800 nm. The absorbance spectra are shown in Figure 14. ZnO nanoparticles are transparent in the visible range inducing a flat curve and highly absorbed in the ultraviolet region.[31] The absorbance of ZnO powders increased with the decrease of precursor concentrations. This may be caused due to the reduction of

https://doi.org/10.1021/acsomega.2c00530
ACS Omega 2022, 7, 31658−31666

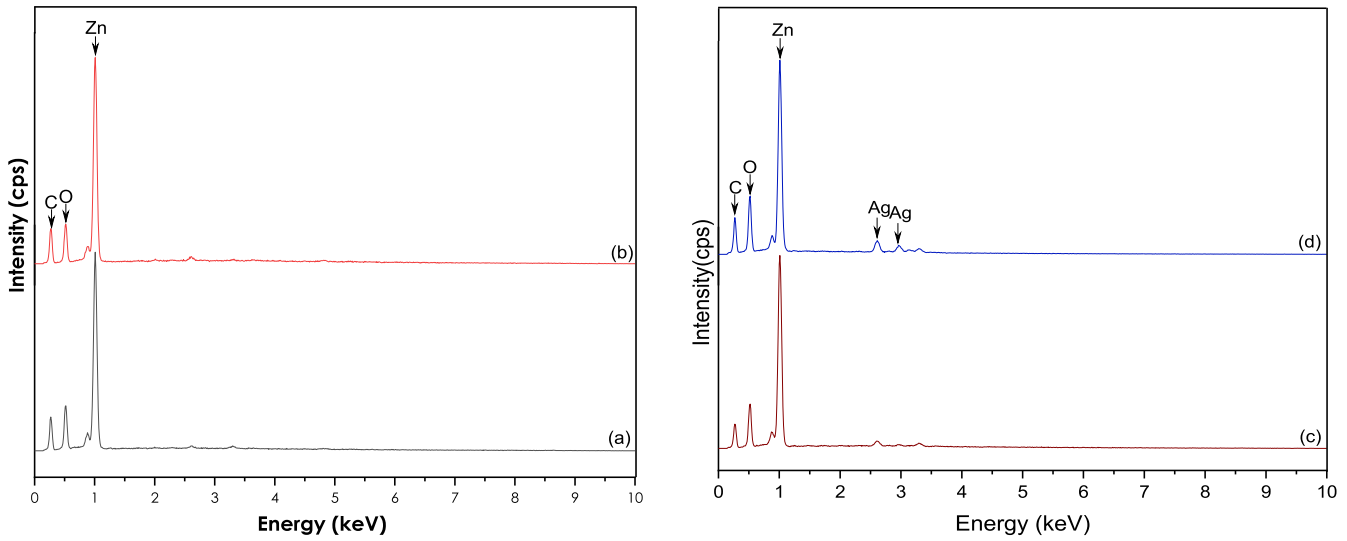

Figure 13. EDS spectra of ZnO nanoparticles doped with (a) 1 and (b) 2% Ce and (c) 1 and (d) 2% Ag.

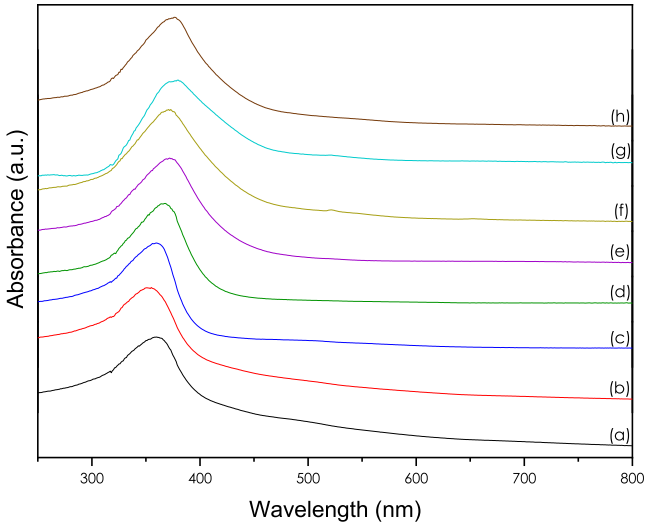

Figure 14. UV−vis spectra of ZnO nanoparticles synthesized using (a) 0.05, (b) 0.1, (c) 0.5, (d) 1, (e) 2, (f) 3, (g) 4, and (h) 5 g of the precursor.

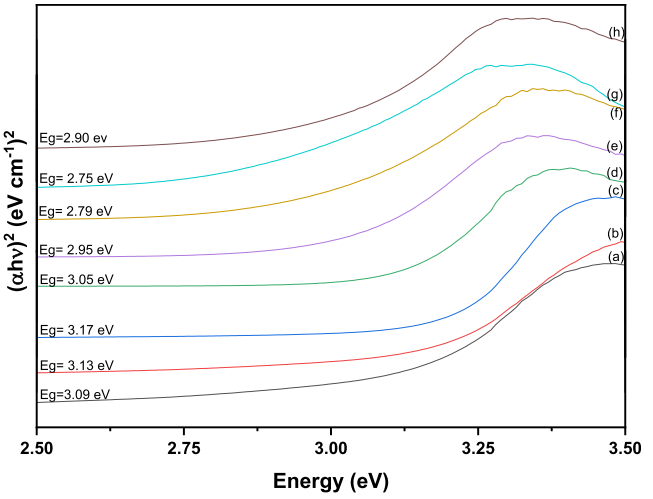

Figure 15. Tauc plot of the optical absorbance spectra of the ZnO nanoparticles synthesized using (a) 0.05, (b) 0.1, (c) 0.5, (d) 1, (e) 2, (f) 3, (g) 4, and (h) 5 g of the precursor.

particle size when the precursor is reduced. These findings were confirmed by Barreto et al. in the microwave-assisted synthesis of ZnO nanoparticles[32] and were following the XRD results. The band gap energy varied between 2.75 and 3.17 eV as calculated using the Tauc plot (Figure 15), with some variations due to the amount of precursor used during the synthesis. However, the literature suggests that ZnO nanoparticles present wide band gap energy of 3.3 eV and a large binding energy of 60 meV at room temperature.[33]

The band gap energy of ZnO nanoparticles was increased with the augmentation of the annealing temperature. The estimation from the Tauc plot showed that the band gap (E_g) was 3.00 and 3.16 eV when annealed using 600 and 800 °C, respectively (Figure 16). The results of the excitation and inter-transition properties of ZnO nanoparticles annealed at 600 and 800 °C show a peak shift from 367 to 369 nm, in this case, due to the annealing temperatures as presented in Figure 15. Many variables such as the change of particle size, structural characteristics, or the presence of certain contaminants can be the cause of this change.[34]

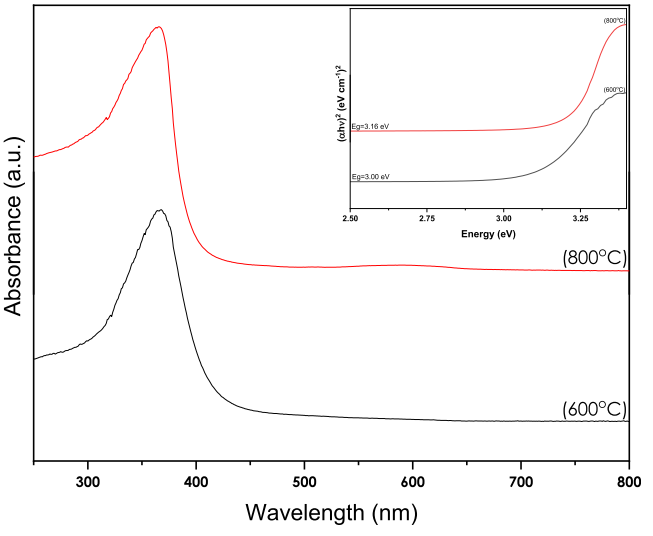

Figure 16. UV−vis spectra of ZnO nanoparticles annealed at (a) 600 and (b) 800 °C.

https://doi.org/10.1021/acsomega.2c00530
ACS Omega 2022, 7, 31658−31666

UV−vis spectra of ZnO and Ce-doped ZnO show a peak shift to longer wavenumbers with the augmentation of the dopant concentration, as presented in Figure 17. The

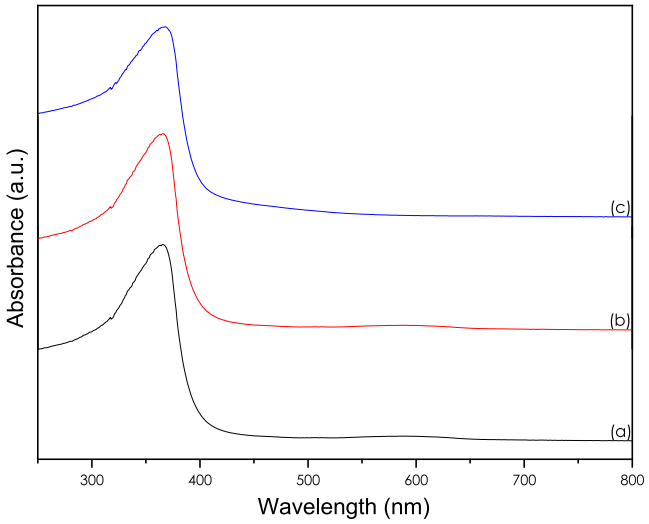

Figure 17. UV−vis pattern of (a) pure ZnO nanoparticles and doped with (b) 1 and (c) 2% cerium.

absorption shift to the longer wavelength region is caused by cerium doping, which creates oxygen vacancies and additional energy levels. The shift can be attributed to the formation of shallow-level ZnO nanoparticles within the band gap as a result of Ce^{3+} ions introduced into the wurtzite ZnO lattice.[26] The band gap energies of Ce-doped ZnO nanoparticles were 3.19 and 3.20 eV for 2 and 1% dopant, respectively, thus increasing the band gap energy compared to the undoped ZnO nanoparticles.

The shift of the absorption peak represents changes in the particles' energy band gap due to the incorporation of Ag^{+} ions into the ZnO nanoparticle lattice.[28] The Ag-doped peak was observed at 370 nm and presented a red shift toward the higher wavelength. Optical absorption spectra of pure ZnO powder and Ag-doped ZnO is presented in Figure 18. Doping

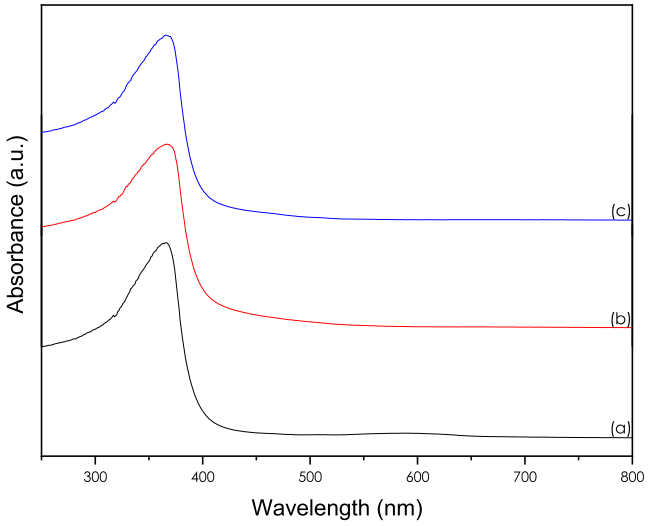

Figure 18. UV−vis pattern of (a) pure ZnO nanoparticles and doped with (b) 1 and (c) 2% Ag.

with Ag increased the band gap energy of ZnO nanoparticles; however, the doping concentration did not induce any changes in the band gap energy level that remained at 3.19 eV for both 1 and 2% Ag dopant concentration as shown in Figure 19.

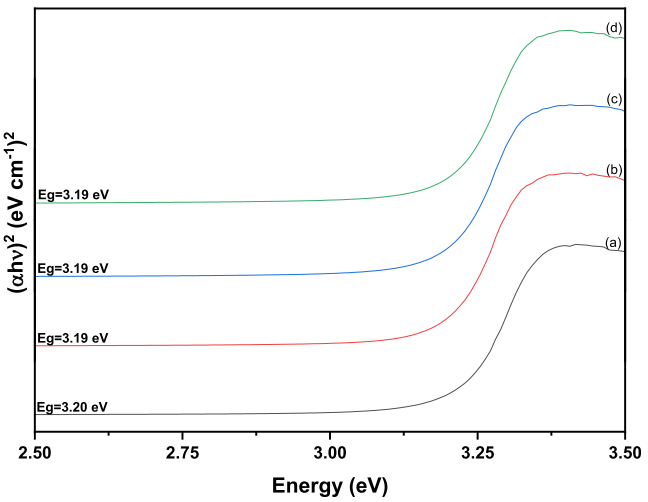

Figure 19. Band gap energy and Tauc plot of the optical absorbance spectra of the ZnO nanoparticles doped with (a) 1 and (b) 2% cerium, and (c) 1 and (d) 2% silver.

4. CONCLUSIONS

The study demonstrated that pure ZnO nanoparticles of high grade were obtained by an entirely green chemistry process using bush tea leaf extract as a reducing agent and zinc nitrate hexahydrate as the precursor. The calculation of the crystallite size using the Scherrer equation showed that the Al size of ZnO nanoparticles synthesized using different precursor concentrations was ranging between 24.53 and 63.02 nm. The EDS and FTIR analyses confirmed the formation of pure ZnO nanoparticles. The increase in precursor concentration tends to increase the purity levels of formed nanoparticles. SEM measurements showed that ZnO nanoparticles were quasi-spherical with some exceptions when doping with 2% Ce and Ag where nanorods were found to be formed. This demonstrated that the size distribution of particles was uniform. The increase in both dopants was found to leave extra Ce and Ag that did not integrate with the ZnO nanoparticle lattice.

AUTHOR INFORMATION

Corresponding Author

Shohreh Azizi − *UNESCO-UNISA Africa Chair in Nanoscience and Nanotechnology College of Graduates Studies, University of South Africa, Pretoria 392, South Africa; Nanosciences African Network (NANOAFNET), iThemba LABS-National Research Foundation, Somerset West 7129 Western Cape, South Africa;* orcid.org/0000-0003-0419-9953; Email: shohrehazizi1379@gmail.com

Authors

Amani Gabriel Kaningini − *UNESCO-UNISA Africa Chair in Nanoscience and Nanotechnology College of Graduates Studies, University of South Africa, Pretoria 392, South Africa; Nanosciences African Network (NANOAFNET), iThemba LABS-National Research Foundation, Somerset*

https://doi.org/10.1021/acsomega.2c00530
ACS Omega 2022, 7, 31658−31666

West 7129 Western Cape, South Africa; orcid.org/0000-0003-3849-8011

Nolufundo Sintwa − *UNESCO-UNISA Africa Chair in Nanoscience and Nanotechnology College of Graduates Studies, University of South Africa, Pretoria 392, South Africa; Nanosciences African Network (NANOAFNET), iThemba LABS-National Research Foundation, Somerset West 7129 Western Cape, South Africa*

Kagiso Mokalane − *Nanotechnology and Water Sustainability Research (NanoWS) Unit, College of Science, Engineering and Technology, University of South Africa, Johannesburg 1709, South Africa*

Keletso Cecilia Mohale − *Department of Agriculture and Animal Health, College of Agriculture and Environmental Sciences, University of South Africa, Florida 1710, South Africa*

Fhatuwani Nixwell Mudau − *Department of Agriculture and Animal Health, College of Agriculture and Environmental Sciences, University of South Africa, Florida 1710, South Africa; School of Agricultural, Earth and Environmental Sciences, University of KwaZulu-Natal, Pietermaritzburg 3201, South Africa*

Malik Maaza − *UNESCO-UNISA Africa Chair in Nanoscience and Nanotechnology College of Graduates Studies, University of South Africa, Pretoria 392, South Africa; Nanosciences African Network (NANOAFNET), iThemba LABS-National Research Foundation, Somerset West 7129 Western Cape, South Africa*

Complete contact information is available at: https://pubs.acs.org/10.1021/acsomega.2c00530

Notes

The authors declare no competing financial interest.

■ ACKNOWLEDGMENTS

The authors are extremely grateful to the Department of Agriculture and Animal Health of the University of South Africa and the Unesco-Unisa Africa Chair for Nanosciences and Nanotechnology for their financial support.

■ REFERENCES

(1) Gunalan, S.; Sivaraj, R.; Rajendran, V. Green Synthesized ZnO Nanoparticles against Bacterial and Fungal Pathogens. *Prog. Nat. Sci.: Mater. Int.* **2012**, *22*, 693−700.

(2) Jamdagni, P.; Khatri, P.; Rana, J. S. Green Synthesis of Zinc Oxide Nanoparticles Using Flower Extract of Nyctanthes Arbor-Tristis and Their Antifungal Activity. *J. King Saud Univ.* **2018**, *30*, 168−175.

(3) Zhao, J.; Shao, Q.; Ge, S.; Zhang, J.; Lin, J.; Cao, D.; Wu, S.; Dong, M.; Guo, Z. Advances in Template Prepared Nano-Oxides and Their Applications: Polluted Water Treatment, Energy, Sensing and Biomedical Drug Delivery. *Chem. Rec.* **2020**, *20*, 710−729.

(4) Sharma, S.; Kumar, S.; Bulchandini, B.; Taneja, S.; Banyal, S. Green Synthesis of Silver Nanoparticles and Their Antimicrobial Activity against Gram Positive and Gram Negative Bacteria. *Int. J. Biotechnol. Bioeng Res.* **2013**, *4*, 341−346.

(5) Koupaei, M. H.; Shareghi, B.; Saboury, A. A.; Davar, F.; Semnani, A.; Evini, M. Green Synthesis of Zinc Oxide Nanoparticles and Their Effect on the Stability and Activity of Proteinase K. *RSC Adv.* **2016**, *6*, 42313−42323.

(6) Pholnak, C.; Sirisathitkul, C.; Suwanboon, S.; Harding, D. J. Effects of Precursor Concentration and Reaction Time on Sonochemically Synthesized ZnO Nanoparticles. *Mater. Res.* **2014**, *17*, 405−411.

(7) Amirthavalli, C.; Manikandan, A.; Prince, A. A. M. Effect of Zinc Precursor Ratio on Morphology and Luminescent Properties of ZnO Nanoparticles Synthesized in CTAB Medium. *Ceram. Int.* **2018**, *44*, 15290−15297.

(8) Fifere, N.; Airinei, A.; Timpu, D.; Rotaru, A.; Sacarescu, L.; Ursu, L. New Insights into Structural and Magnetic Properties of Ce Doped ZnO Nanoparticles. *J. Alloys Compd.* **2018**, *757*, 60−69.

(9) Sharma, P. K.; Dutta, R. K.; Pandey, A. C.; Layek, S.; Verma, H. C. Effect of Iron Doping Concentration on Magnetic Properties of ZnO Nanoparticles. *J. Magn. Magn. Mater.* **2009**, *321*, 2587−2591.

(10) Behrens, M.; Lolli, G.; Muratova, N.; Kasatkin, I.; Hävecker, M.; d'Alnoncourt, R. N.; Storcheva, O.; Köhler, K.; Muhler, M.; Schlögl, R. The Effect of Al-Doping on ZnO Nanoparticles Applied as Catalyst Support. *Phys. Chem. Chem. Phys.* **2013**, *15*, 1374−1381.

(11) Pradeev Raj, K.; Sadaiyandi, K.; Kennedy, A.; Sagadevan, S.; Chowdhury, Z. Z.; Johan, M. R. B.; Aziz, F. A.; Rafique, R. F.; Thamiz Selvi, R.; Rathina Bala, R. Influence of Mg Doping on ZnO Nanoparticles for Enhanced Photocatalytic Evaluation and Anti-bacterial Analysis. *Nanoscale Res. Lett.* **2018**, *13*, 229.

(12) Iravani, S.; Korbekandi, H.; Zolfaghari, B. Phytosynthesis of Nanoparticles. *Nanotechnol. Plant Sci.* **2015**, 203−258.

(13) Thema, F. T.; Manikandan, E.; Dhlamini, M. S.; Maaza, M. Green Synthesis of ZnO Nanoparticles via Agathosma Betulina Natural Extract. *Mater. Lett.* **2015**, *161*, 124−127.

(14) Latif, M. S.; Abbas, S.; Kormin, F.; Mustafa, M. K. Green Synthesis of Plant-Mediated Metal Nanoparticles: The Role of Polyphenols. *Asian J. Pharm. Clin. Res.* **2019**, *12*, 75−84.

(15) Sahu, N.; Soni, D.; Chandrashekhar, B.; Satpute, D. B.; Saravanadevi, S.; Sarangi, B. K.; Pandey, R. A. Synthesis of Silver Nanoparticles Using Flavonoids: Hesperidin, Naringin and Diosmin, and Their Antibacterial Effects and Cytotoxicity. *Int. Nano Lett.* **2016**, *6*, 173−181.

(16) Tshikhudo, P. P.; Ntushelo, K.; Kanu, S. A.; Mudau, F. N. Growth Response of Bush Tea (Athrixia Phylocoides DC.) to Climatic Conditions in Limpopo Province, South Africa. *South Afr. J. Bot.* **2019**, *121*, 500−504.

(17) Lerotholi, L.; Chaudhary, S. K.; Combrinck, S.; Viljoen, A. Bush Tea (Athrixia Phylicoides): A Review of the Traditional Uses, Bioactivity and Phytochemistry. *South Afr. J. Bot.* **2017**, *110*, 4−17.

(18) Mudau, F. N.; Ngezimana, W. Effect of Different Drying Methods on Chemical Composition and Antimicrobial Activity of Bush Tea (Athrixia Phylicoides). *Int. J. Agric. Biol.* **2014**, *16*, 1011.

(19) Ranoszek-Soliwoda, K.; Tomaszewska, E.; Socha, E.; Krzyczmonik, P.; Ignaczak, A.; Orlowski, P.; Krzyzowska, M.; Celichowski, G.; Grobelny, J. The Role of Tannic Acid and Sodium Citrate in the Synthesis of Silver Nanoparticles. *J. Nanoparticle Res.* **2017**, *19*, 273.

(20) Lopes, L. D.; Pereira e Silva, M. d. C.; Weisberg, A. J.; Davis, E. W.; Yan, Q.; Varize, C. d. S.; Wu, C. F.; Chang, J. H.; Loper, J. E.; Andreote, F. D. Genome Variations between Rhizosphere and Bulk Soil Ecotypes of a Pseudomonas Koreensis Population. *Environ. Microbiol.* **2018**, *20*, 4401−4414.

(21) Kamaruzaman, A.; Lah, N. A. C. Formation of ZnO Nanoparticles in the Presence of Tannic Acid. *Environ. Microbiol.* **2021**, *41*, 61−64.

(22) Matinise, N.; Fuku, X. G.; Kaviyarasu, K.; Mayedwa, N.; Maaza, M. ZnO Nanoparticles via Moringa Oleifera Green Synthesis: Physical Properties & Mechanism of Formation. *Appl. Surf. Sci.* **2017**, *406*, 339−347.

(23) Olivier, J.; Symington, E. A.; Jonker, C. Z.; Van Eeden, T. S.; Rampedi, I. T. Comparison of the Mineral Composition of Leaves and Infusions of Traditional and Herbal Teas. *S. Afr. J. Anim. Sci.* **2012**, *108*, 1−7.

(24) Monshi, A.; Foroughi, M. R.; Monshi, M. R. Modified Scherrer Equation to Estimate More Accurately Nano-Crystallite Size Using XRD. *World J. Nano Sci. Eng.* **2012**, *2*, 154−160.

(25) Uthirakumar, P.; Hong, C.-H. Effect of Annealing Temperature and PH on Morphology and Optical Property of Highly Dispersible ZnO Nanoparticles. *Mater. Charact.* **2009**, *60*, 1305−1310.

(26) Bomila, R.; Srinivasan, S.; Venkatesan, A.; Bharath, B.; Perinbam, K. Structural, Optical and Antibacterial Activity Studies of Ce-Doped ZnO Nanoparticles Prepared by Wet-Chemical Method. *Mater. Res. Innovat.* **2018**, *22*, 379−386.
(27) Nigussie, G. Y.; Tesfamariam, G. M.; Tegegne, B. M.; Weldemichel, Y. A.; Gebreab, T. W.; Gebrehiwot, D. G.; Gebremichel, G. E. Antibacterial Activity of Ag-Doped TiO2 and Ag-Doped ZnO Nanoparticles. *Int. J. Photoenergy* **2018**, 5927485.
(28) Hosseini, S. M.; Sarsari, I. A.; Kameli, P.; Salamati, H. Effect of Ag Doping on Structural, Optical, and Photocatalytic Properties of ZnO Nanoparticles. *J. Alloys Compd.* **2015**, *640*, 408−415.
(29) Nethavhanani, T. Synthesis of Zinc Oxide Nanoparticles by a Green Process and the Investigation of Their Physical Properties. *AIP Conf. Proc.* **2018**, *1962*, 040007.
(30) Fakhari, S.; Jamzad, M.; Kabiri Fard, H. Green Synthesis of Zinc Oxide Nanoparticles: A Comparison. *Green Chem. Lett. Rev.* **2019**, *12*, 19−24.
(31) Baneto, M.; Enesca, A.; Lare, Y.; Jondo, K.; Napo, K.; Duta, A. Effect of Precursor Concentration on Structural, Morphological and Opto-Electric Properties of ZnO Thin Films Prepared by Spray Pyrolysis. *Ceram. Int.* **2014**, *40*, 8397−8404.
(32) Barreto, G. P.; Morales, G.; Quintanilla, M. L. L. Microwave Assisted Synthesis of ZnO Nanoparticles: Effect of Precursor Reagents, Temperature, Irradiation Time, and Additives on Nano-ZnO Morphology Development. *J. Mater.* **2013**, *2013*, 1−11.
(33) Kolekar, T. V.; Yadav, H. M.; Bandgar, S. S.; Deshmukh, P. Y. Synthesis by Sol−Gel Method and Characterization of ZnO Nanoparticles. *Indian Streams Res. J.* **2011**, *1*, 1−4.
(34) Verma, N.; Bhatia, S.; Bedi, R. K. Effect of Annealing Temperature on ZnO Nanoparticles and Its Applications for Photocatalytic Degradation of DR-31 Dye. *Int. J. Pure Appl. Phys.* **2017**, *13*, 118−122.

https://doi.org/10.1021/acsomega.2c00530
ACS Omega 2022, 7, 31658−31666